Spin Squeezing

by

Trent Fridey

A thesis submitted to the faculty of the

University of Colorado in partial fulfillment

of the requirements for the award of

departmental honors in the Department of Physics

2014

This thesis entitled:
Spin Squeezing
written by Trent Fridey
has been approved for the Department of Physics

Ana Maria Rey

Prof. John Cumalat

Prof. Alejandro Sarria

Date

The final copy of this thesis has been examined by the signatories, and we find that both the content and the form meet acceptable presentation standards of scholarly work in the above mentioned discipline.

Fridey, Trent (B.A., Physics)

Spin Squeezing

Thesis directed by Prof. Ana Maria Rey

Defended on Nov. 4th, 2014

Contemporary experimental research in the field of atomic, molecular, and optical physics has made great progress in establishing fully controllable ultracold atomic systems. Applications of these controllable systems include precise atomic clocks [1] and quantum simulation [2]. Examples of controllable atomic systems include trapped ions [3], atomic systems interacting via the dipole-dipole interaction [4], and atoms trapped in optical lattices with superexchange interactions [5]. These systems have the potential to realize spin squeezing. Advancements in trapped ion experiments have led to control of long-range interactions between the ions. An interesting question to ask is how to maximize spin squeezing in these systems. The purpose of this thesis, therefore, is to analyze the effect that the range of the interactions has on spin squeezing. Numerical simulations are used to gain insight into the maximum amount of spin squeezing that can be generated. Throughout this thesis, Ramsey spectroscopy will be used as an example to understand potential applications of spin squeezing.

Dedication

This thesis is dedicated to my parents for their unconditional love and support.

Acknowledgements

I thank and acknowledge my advisor, Ana Maria Rey, for teaching me a tremendous amount about the theory of quantum mechanics. Specifically, I am not only indebted for her code in implementing operators in large Hilbert spaces, but also for the time she took for many discussions with me over the course of this work.

I also acknowledge the other members of the Rey group for helpful discussions.

Contents

Chapter

Figures

Figure

Chapter 1

Introduction

Contemporary experimental research in the field of atomic, molecular, and optical physics has made great progress in establishing fully controllable ultracold atomic systems. There are many applications of these systems. For example, atomic clocks use the internal quantized levels of atoms to set the universal time standard [1]. These atomic systems are much better than mechanical systems because of the control that exists over the many degrees of freedom. In addition, atomic systems are useful in the domain of quantum simulation, where atoms trapped in an optical lattice simulate the behavior of electrons in a physical lattice [2]. The key to quantum simulation is the interaction of the atoms. This and the control over the many degrees of freedom in these systems motivates the study of spin squeezing in this context [6].

As quantum systems, atomic clocks possess a fundamental amount of uncertainty in their operation. Quantum systems are inevitably constrained by an uncertainty principle. For example, the resolution in the position, ΔX, of a quantum particle and resolution in the momentum, ΔP, of the same particle are constrained such that their product is always greater than half of Planck's constant, $\hbar$. This puts a limit on the maximum simultaneous resolution of the position and momentum of the quantum particle. Likewise, the projection of the axis of rotation of a quantum particle along three orthogonal axes (the components of the spin axes), denoted $\hat{S}^x, \hat{S}^y,$ and $\hat{S}^z$, can only be resolved such that the product of uncertainties of two orthogonal projections are greater than the expectation value of the projection on the third axis. For example,

$$(\Delta S^y)(\Delta S^z) \geq \frac{\hbar}{2}\left|\langle \hat{S}^x \rangle\right| \tag{1.1}$$

This statement of uncertainty can limit the precision of the atomic clock. There are several ways to increase the precision of an atomic clock at this limit. As will be explained later, one can reduce the uncertainty by using more quantum particles during the measurement process. A better method is to employ spin squeezing. For a system where the uncertainty relation is saturated, one can decrease ΔS^z by increasing ΔS^y. This system is considered "spin-squeezed"–we have reduced a quantity along one axis and this has resulted in the quantity along an orthogonal axis becoming bloated.

Systems of trapped ions [3], atomic systems interacting via the dipole-dipole interaction [4], and atoms trapped in optical lattices with superexchange interactions [5] have the potential to realize spin squeezing. Advancements in trapped ion experiments have led to control of long-range interactions between the ions. The purpose of this thesis is to analyze the effect that the range of the interactions have on the potential spin squeezing. Numerical simulations are used to gain insight into the maximum amount of spin squeezing that can be generated, and Ramsey spectroscopy is introduced to understand the potential applications of spin squeezing.

Chapter 2

Mathematical Background

2.1 Spin-1/2 and the Bloch Sphere

Quantum particles have an intrinsic angular momentum called spin. The spin of a particle in quantum mechanics is quantized such that the projection of the vector describing its axis of rotation along any spatial axis is an integer multiple of $\hbar/2$. A spin with the fundamental quantum of spin is called a spin-1/2 particle. The spin state is described by a state vector, $|\psi\rangle$, in Hilbert space. The components of the spin along the three spatial axes for a spin-1/2 particle are given by the components of the vector $\langle\hat{\sigma}\rangle = \{\langle\psi|\,\hat{\sigma}^x\,|\psi\rangle\,, \langle\psi|\,\hat{\sigma}^y\,|\psi\rangle\,, \langle\psi|\,\hat{\sigma}^z\,|\psi\rangle\}$, where

$$\hat{\sigma}^x = \begin{pmatrix} 0 & 1 \\ 1 & 0 \end{pmatrix}, \qquad \hat{\sigma}^y = \begin{pmatrix} 0 & -i \\ i & 0 \end{pmatrix}, \qquad \hat{\sigma}^z = \begin{pmatrix} 1 & 0 \\ 0 & -1 \end{pmatrix}, \tag{2.1}$$

and the values for the components are bounded within the range $[-1, 1]$. The state is an eigenstate of the spin operator $\hat{S}^2 = (1/4)((\hat{\sigma}^x)^2 + (\hat{\sigma}^y)^2 + (\hat{\sigma}^z)^2)$ with eigenvalue of 3/4. The requirements that the spin is a eigenstate of $\hat{S}^2$ and the components $\langle\hat{\sigma}^x\rangle\,, \langle\hat{\sigma}^y\rangle\,,$ and $\langle\hat{\sigma}^z\rangle$ are bounded between -1 and 1, suggest that the state $|\psi\rangle$ can be visualized as a vector constrained to the surface a sphere of radius one. This sphere is referred to as the Bloch sphere, and it is a helpful visual tool for relating the spin state $|\psi\rangle$ of a spin-1/2 particle to its projections along the three orthogonal axes. The Bloch vector, $\mathbf{n}$, is defined for a spin state $|\psi\rangle$ such that $|\psi\rangle$ is the eigenstate of the operator $\mathbf{n}\cdot\hat{\sigma}$. The Bloch vector for the state $|-z\rangle$, is represented in figure (2.1). The Bloch vector points along the direction of the expectation value of $\hat{\sigma}$ [7].

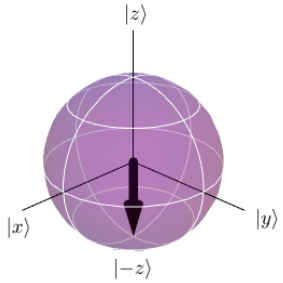

Figure 2.1: Bloch sphere with a spin-1/2 particle whose Bloch vector is pointing down on the z-axis.

The state $|x\rangle$ is the notation for the eigenstate of $\mathbf{n} \cdot \hat{\sigma}$ with $\mathbf{n} = \mathbf{x}$. The state $|y\rangle$ is the notation for the eigenstate of $\mathbf{n} \cdot \hat{\sigma}$ with $\mathbf{n} = \mathbf{y}$. A general state on the Bloch sphere can be built out of the superposition of $|z\rangle$ and $|-z\rangle$ by specifying two angles, θ, the polar angle, and ϕ, the azimuthal angle, to describe its location on the sphere. Hence the general state $|\psi\rangle$ on the Bloch sphere is given by:

$$|\psi\rangle = \cos\left(\frac{\theta}{2}\right)|-z\rangle + e^{i\phi}\sin\left(\frac{\theta}{2}\right)|+z\rangle \tag{2.2}$$

It should be noted that, because quantum mechanics allows for superposition of states with a relative complex phase between them, any two orthonormal states (a "two level system") can be used in place of $|z\rangle$ and $|-z\rangle$. In the context of atomic clocks, the two states are the ground state $|g\rangle$ and the excited state $|e\rangle$ of the atom's electron. The corresponding Bloch sphere for these systems is shown in figure (2.2).

The generalized spin operators can then be expressed in terms of projection operators:

$$\hat{\sigma}^x = (|e\rangle\langle g| + |g\rangle\langle e|) \tag{2.3}$$

$$\hat{\sigma}^y = -i(|e\rangle\langle g| - |g\rangle\langle e|) \tag{2.4}$$

$$\hat{\sigma}^z = |e\rangle\langle e| - |g\rangle\langle g| \tag{2.5}$$

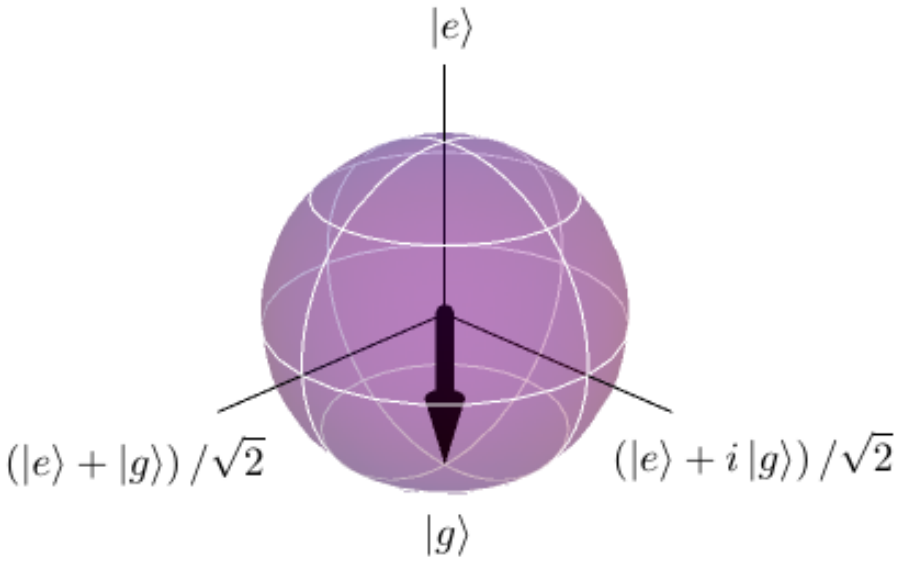

Figure 2.2: The Bloch sphere formed by using the electronic degrees of freedom of an atom in an atomic clock

2.2 Ramsey Spectroscopy

Ramsey spectroscopy applies separated oscillatory fields to atoms to generate an atomic clock. One typically uses an ensemble of many atoms, but for the sake of illustration, consider using a single atom. Start with an atom in state $|g\rangle$, that is, with the Bloch vector pointing down along the z-axis of the Bloch sphere. One then applies a rotation of the vector about the y-axis of the Bloch sphere by applying a microwave pulse of frequency, Ω, for a time, t, on the atom such that $\Omega t = \pi/2$. The Hamiltonian for this pulse is $\hat{H} = \Omega\hat{\sigma}^y$. This places the state along the x-axis of the Bloch sphere. The state then precesses about the z-axis in the xy-plane for a time, τ, due to the detuning, δ, in the laser frequency. The Hamiltonian governing this evolution can be written as $\hat{H} = \delta\hat{\sigma}^z$. Finally, the state is flipped onto the xz-plane of the Bloch sphere by rotating the state about the y-axis with another microwave pulse as before with $\Omega t = \pi/2$, and then the z-component of the Bloch vector, $\hat{\sigma}^z$, is measured. This measurement yields the expectation value

$$\langle\hat{\sigma}^z(\tau)\rangle = \cos(\delta\tau) \tag{2.6}$$

where $\delta = \omega - \omega_0$ is the detuning of the laser frequency, ω, from the atomic transition frequency ω_0. The idea for an atomic clock is to lock onto the atomic transition frequency [8]. The general procedure of Ramsey spectroscopy is illustrated by figure (2.3). An example of the oscillation of the z-component of the Bloch vector due to the detuning of the laser is shown in figure (2.4).

An atomic clock operated by the Ramsey sequence has a laser that is locked on to the atomic transition frequency. The quality of the operation in this case is based on how small the error in the laser frequency is [6]. From the standard error propagation formula, the uncertainty in the detuning is given by:

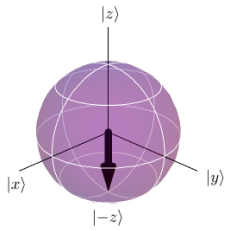

(a) At the beginning of the sequence, the state points along the z-axis of the Bloch sphere.

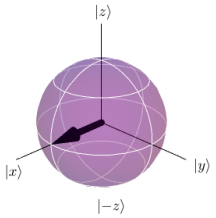

(b) After the first $\pi/2$-pulse, the state is rotated by an angle $\pi/2$ about the y-axis.

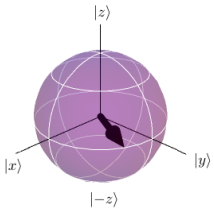

(c) The state then precesses in the xy-plane for a time τ.

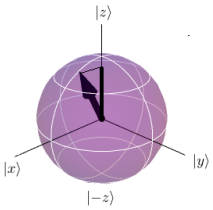

(d) After the final pulse, the state is flipped into the xz-plane, and the z-component of the spin is measured.

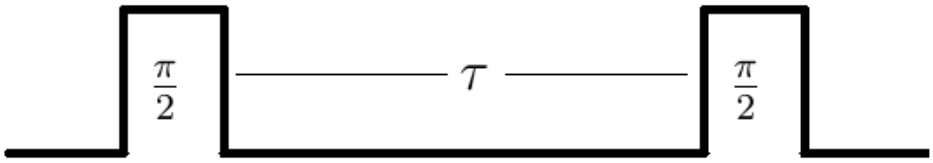

(e) Laser pulses corresponding to the Ramsey sequence

Figure 2.3: Ramsey spectroscopy of one spin-1/2 particle.

Figure 2.4: The z-component of the spin after the final pulse of the Ramsey sequence.

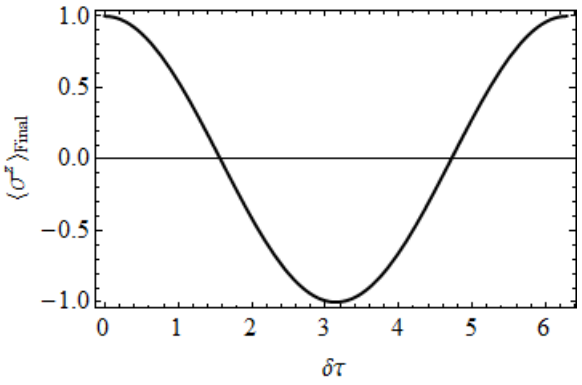

$$\Delta\sigma^z = \left|\frac{\partial\langle\hat{\sigma}^z\rangle}{\partial\delta}\right|\Delta\delta \tag{2.7}$$

$$\frac{\partial\langle\hat{\sigma}^z\rangle}{\partial\delta} = -\tau\sin(\delta\tau) \tag{2.8}$$

$$\Delta\sigma^z = \sin(\delta\tau) \tag{2.9}$$

$$\implies \Delta\delta = 1/\tau \tag{2.10}$$

Therefore, the quality of Ramsey spectroscopy for one spin can be limited by the time of free precession.

2.3 From One Spin to Many Spins

The benefit of using many spins instead of one spin is that, at the end of the Ramsey sequence, the uncertainty in the measurement is decreased by a factor $1/\sqrt{N}$, for a measurement using N spins. This scaling is called the projection-noise limit, or Standard Quantum Limit (SQL). This limit holds for uncorrelated spins, but by using correlated spins one can have the original uncertainty decrease by up to a factor of $1/N$, which is the so-called Heisenberg limit. By extending Ramsey spectroscopy to many spins, one can derive the Heisenberg limit and gain insight into how to reach it experimentally. Let us begin by generalizing the notion of the Bloch sphere and Bloch vector to an ensemble of spin-1/2.

Consider a collection of spin-1/2 systems, which could describe atoms with two electronic states. The i^{th} spin is described by equation (2.2) with the two angles denoted as $\theta = \theta_i$ and $\phi = \phi_i$. In order to describe the state, $|\psi\rangle$, of the collection of spin states, we take the direct product over all states.

$$|\psi\rangle = \bigotimes_{i=1}^{N}\left(\cos\left(\frac{\theta_i}{2}\right)|-z\rangle_i + e^{i\phi_i}\sin\left(\frac{\theta_i}{2}\right)|z\rangle_i\right) \tag{2.11}$$

In this state, we have a collection of spins pointing in random directions on individual Bloch spheres. In the case that all the spins are pointing along the same direction, that is $\theta_i = \theta$ and

$\phi_i = \phi$, the state is called a coherent spin state (CSS), denoted by $|\theta, \phi\rangle$. This is an important state for performing Ramsey spectroscopy on an ensemble of spin-1/2, as will be discussed later.

The collective spin operators for a system of many spins are sums of the single-spin operators. The single-spin operators only operate on single spins. Explicitly, the collective spin operators are:

$$\hat{S}^x = \frac{1}{2}\sum_{i=1}^{N} \hat{\sigma}_i^x \tag{2.12}$$

$$\hat{S}^y = \frac{1}{2}\sum_{i=1}^{N} \hat{\sigma}_i^y \tag{2.13}$$

$$\hat{S}^z = \frac{1}{2}\sum_{i=1}^{N} \hat{\sigma}_i^z \tag{2.14}$$

Using these operators, the CSS can be visualized on a generalized Bloch sphere with a generalized Bloch vector. For instance, by following ref. [9], one can derive the identities:

$$\langle\theta, \phi| \hat{S}^x |\theta, \phi\rangle = S\cos(\phi)\sin(\theta) \tag{2.15}$$

$$\langle\theta, \phi| \hat{S}^y |\theta, \phi\rangle = S\sin(\phi)\sin(\theta) \tag{2.16}$$

$$\langle\theta, \phi| \hat{S}^z |\theta, \phi\rangle = S\cos(\theta) \tag{2.17}$$

Here S is the total spin, which for a system with N spin-1/2, is equal to $N/2$. Equation (2.15) then describes a Bloch vector with length S. Because one can describe the many-spin state in the same way as the single spin state, and because the collective spin operators are sums of spin operators which act only on single particles, the Ramsey sequence described in the previous section works for either an ensemble of spin-1/2 or for a single spin-1/2.

A useful tool to visualize the CSS is the Husimi Q-function. Given a specific CSS, such as the $\left|\theta = \frac{\pi}{2}, \phi = 0\right\rangle$, the Q-function of this state is given by projecting this state onto the general CSS:

$$Q(\theta, \phi) = |\langle\theta, \phi \mid \theta = \pi/2, \phi = 0\rangle|^2 \tag{2.18}$$

The utility of this function is that it is similar to a probability distribution when plotted on a sphere. Not only does it show the direction of the generalized Bloch vector (referred to as the "mean spin direction"), but it also shows the distribution of noise on the generalized Bloch sphere due to quantum fluctuations. The Q-function for the CSS with $\theta = \pi/2$ and $\phi = 0$ is shown in figure (2.5)

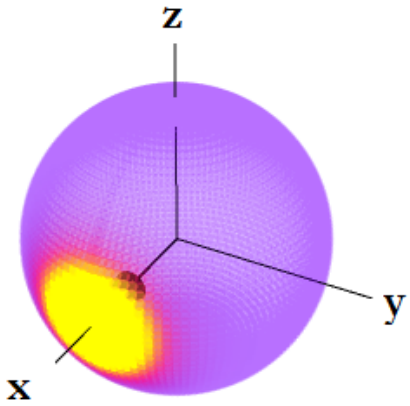

Figure 2.5: The Q-function for the CSS with $\theta = \pi/2$ and $\phi = 0$, with a vector denoting the mean spin direction. The yellow-colored region denotes the uncertainty in the components of the spin vector transverse to the mean spin direction.

At the beginning of the chapter, it was claimed that the uncertainty in the measurement at the end of a Ramsey sequence decreases with the number of particles, N, like $1/\sqrt{N}$. To rigorously justify the uncertainty, consider the error analysis done for the detuning in Ramsey spectroscopy for one spin-1/2. The idea that was used to derive the uncertainty in the detuning for one spin can be used again for the case of many spins.

$$\Delta\sigma^z = \left|\frac{\partial\langle\hat{\sigma}^z\rangle}{\partial\delta}\right|\Delta\delta \tag{2.19}$$

$$\frac{\partial\langle\hat{\sigma}^z\rangle}{\partial\delta} = -(N/2)\tau\sin(\delta\tau) \tag{2.20}$$

$$\Delta\sigma^z = (\sqrt{N}/2)\sin(\delta\tau) \tag{2.21}$$

$$\implies \Delta\delta = 1/(\sqrt{N}\tau) \tag{2.22}$$

This is the benefit of using an ensemble of spins over a single spin for Ramsey spectroscopy, because increasing the number of spins used decreases the uncertainty in the detuning by a factor of $1/\sqrt{N}$. But as alluded to before, there exists a better limit, the Heisenberg limit, where the uncertainty in the detuning in Ramsey spectroscopy scales like $1/N$. The Heisenberg limit follows from the energy-time uncertainty relation in quantum mechanics. The principle states that, for a time interval δt during which a measurement of the Hamiltonian is made, the variance of the Hamiltonian, ΔH^2, is constrained such that

$$\delta t^2 \Delta H^2 \geq \frac{1}{4} \tag{2.23}$$

Following ref. [10], this inequality can be rewritten in terms of a dimensionless phase $\delta\varphi$, and the operator $\hat{\sigma}^z = \sum_i \hat{\sigma}_i^z$. We can also place an upper bound on the value of $(\Delta\hat{\sigma}^z)^2$ because the maximum eigenvalue of this operator for N spin-1/2 is $N^2/4$. This implies that the minimum phase interval to distinguish two different states has a lower limit of $\delta\varphi = \frac{1}{N}$, which is referred to as the Heisenberg limit. The Heisenberg limit then provides a strict lower bound on the scaling of the uncertainty with the number of spins used. One can interpret the uncertainty in the phase, $\delta\varphi$, using the Q-function for two CSS which have different mean spin directions. The states must be separated by an angle $\delta\varphi$ on the Bloch sphere in order for the Q-functions to avoid overlapping significantly. This idea is presented in figure (2.6).

Figure 2.6: Illustration of the projection noise limit

(a) The resolution limitations of a state for 4 particles. The phase uncertainty dictates that the spin of two systems must be separated by an angle $\Delta\phi$ on the generalized Bloch sphere in order to be distinguishable.

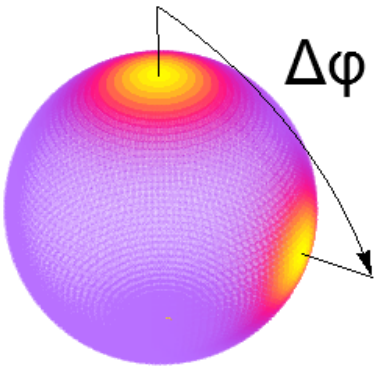

(b) The resolution limitations of a state for 16 particles. From the projection noise limit, the separation of the Q-functions is a factor of 2 smaller than in the previous figure, which means that the minimum distance of separation to distinguish two separate states is much smaller.

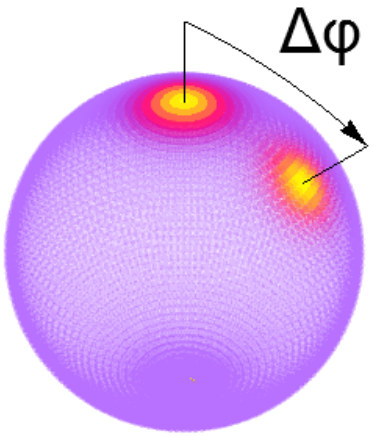

Chapter 3

Methods

3.1 Spin Squeezing

We have already seen how the uncertainty in the detuning in a suitably performed Ramsey sequence depends on the uncertainty in the final measurement of the z-component of the collective spin, and how this uncertainty is constrained by the projection noise limit for the CSS. Spin squeezing is a way to decrease the uncertainty past the projection noise limit. It can involve generating interactions between the spins of the system. In the seminal paper [11], spin squeezing was found to result from an ensemble of spins that were governed by a Hamiltonian $\hat{H} = f(\hat{S}^z) = (\hat{S}^z)^2$, where $\hat{S}^z$ is the collective spin operator along the z-axis. The Hamiltonian must be nonlinear in the collective spin variables in order to generate spin squeezing; Hamiltonians linear in spin operators generate only rotations of the CSS about the generalized Bloch sphere. In order to verify this, it will be helpful to rigorously define the notion of spin squeezing. This is accomplished by defining the spin squeezing parameter, ξ.

3.2 Quantifying Squeezing

We begin our analysis of spin squeezing by the notion of a spin squeezed state (SSS). A spin squeezed state describes the collective spin of a system which has a smaller phase uncertainty than the phase uncertainty for a coherent spin state. Therefore, the uncertainty in the phase for a SSS must compare with the uncertainty in the phase for a CSS such that

$$\frac{\Delta\phi_{SSS}}{\Delta\phi_{CSS}} < 1. \tag{3.1}$$

where $\Delta\phi_{SSS}$ is the phase sensitivity of the squeezed state. The phase uncertainty for a CSS, $\Delta\phi_{CSS}$, is always given by $1/\sqrt{N}$. Hence, one can define an effective squeezing parameter, ξ, in terms of the collective spin components, $\langle\mathbf{S}\rangle$, and the variance of the components of the collective Bloch vector perpendicular to the mean spin direction, $\Delta(\mathbf{S}\cdot\mathbf{n}_\perp)$, such that

$$\xi = \sqrt{N}\Delta\phi_{SSS} = \sqrt{N}\frac{min\Delta(\mathbf{S}\cdot\mathbf{n}_\perp)}{|\langle\mathbf{S}\rangle|}. \tag{3.2}$$

The interpretation of this parameter is as follows: the quantity $\Delta(\mathbf{S}\cdot\mathbf{n}_\perp)$ is the uncertainty of the collective spin components along a normalized vector, $\mathbf{n}_\perp$, which is orthogonal to the mean spin direction. Graphically, $\Delta(\mathbf{S}\cdot\mathbf{n}_\perp)$ can be interpreted as the width of the Q-function distribution on the generalized Bloch sphere. For a spin squeezed state, there will be a special normalized vector, $\mathbf{n}_\perp$, where the uncertainty is the smallest. This means that the Q-function for a SSS is no longer shaped like a circle centered on the mean spin direction, but instead shaped like an ellipse (referred to as the "uncertainty ellipse"). In the definition of the squeezing parameter, this uncertainty is weighted by the magnitude of the collective Bloch vector, so that the squeezing parameter for a CSS equals unity. In order to perform the calculation of the squeezing parameter, we can take a SSS which has a mean spin direction along the x-axis of the generalized Bloch sphere. Then the vector $\mathbf{n}_\perp$ can be parameterized in terms of an angle φ, and two normalized vectors, $\mathbf{y}$ and $\mathbf{z}$, which are orthogonal to the mean spin direction:

$$\mathbf{n}_\perp = \cos(\varphi)\mathbf{y} + \sin(\varphi)\mathbf{z}. \tag{3.3}$$

Inserting this into squeezing parameter definition gives us

$$\xi^2(t) = N\frac{(\Delta S^y)^2\cos^2(\varphi) + (\Delta S^z)^2\sin^2(\varphi) + \left(\frac{1}{2}\langle\{\hat{S}^y,\hat{S}^z\}\rangle + \langle\hat{S}^y\rangle\langle\hat{S}^z\rangle\right)\sin(2\varphi)}{\langle\hat{\mathbf{S}}\rangle^2} \tag{3.4}$$

where $\hat{S}^y$ and $\hat{S}^z$ are the y and z components of the collective spin, and $\{\hat{S}^y, \hat{S}^z\}$ is the anticommutator $\{\hat{S}^y, \hat{S}^z\} = \hat{S}^y\hat{S}^z + \hat{S}^z\hat{S}^y$. The angle, φ, is chosen so that $\mathbf{n}_\perp$ is parallel to the minor axis of the uncertainty ellipse. This corresponds to finding the angle where $\frac{\partial \xi}{\partial \varphi}$ is zero. An extended derivation of this parameter can be found in appendix (A), and we find:

$$\varphi = \frac{1}{2}\tan^{-1}\left[\frac{2\langle \hat{S}^y\rangle\langle \hat{S}^z\rangle - \langle\{\hat{S}^y, \hat{S}^z\}\rangle}{(\Delta S^z)^2 - (\Delta S^y)^2}\right] \tag{3.5}$$

Since the squeezing parameter can be a function of time, then in order to take maximal benefit of the effective squeezing, one should then minimize the squeezing parameter over time. Due to other effects not included in this analysis, such as decoherence, the maximal squeezing is constrained to fall within the first minimum in the time evolution of the parameter, beyond which the mentioned phenomena become relevant [12].

3.3 Effective Hamiltonians and System Geometry

As mentioned previously, in order to generate spin squeezing, there needs to be an effective Hamiltonian that is nonlinear in the collective spin operators. In ref. [3], trapped ions have the potential to realize such a nonlinear Hamiltonian. An example of the application of spin squeezing with trapped ions has already been demonstrated in ref. [13] in the context of Ramsey spectroscopy. In trapped ion systems, the atom's electronic degrees of freedom form the effective spin-1/2 system. By using spin-dependent forces, the ensemble of ions can be made to form a crystal. Other spin-dependent forces, applied through counter-propagating laser fields, generate long-range interactions between the ions. Within this setup, it is possible to generate Hamiltonians of the form:

$$\hat{H}_{OAT} = \sum_{j<k} J_{jk}\hat{\sigma}_j^z\hat{\sigma}_k^z \tag{3.6}$$

$$\hat{H}_{XY} = \sum_{j<k} J_{jk}\left(\hat{\sigma}_j^x\hat{\sigma}_k^x + \hat{\sigma}_j^y\hat{\sigma}_k^y\right) \tag{3.7}$$

$$\tag{3.8}$$

where $\hat{\sigma}_j^z$ is the j^{th} ion's z-component spin operator. The first Hamiltonian is the so-called one-axis-twisting Hamiltonian (denoted by OAT), the second is called the XY model. In trapped ion systems there exists sufficient control that one can engineer the coupling constants J_{jk} between the ions so that the interactions between the atoms form a lattice geometry. Therefore the coupling constants are chosen in this work so that the ions form either a hexagonal lattice or a triangular lattice. These correspond to particle numbers $N = 7$ and $N = 6$ respectively, and are shown in figure (3.1). The embedding of the geometry in the coupling constants is done by defining J_{jk} such that:

$$J_{jk} = \frac{J}{|\mathbf{r}_j - \mathbf{r}_k|^\alpha}, \tag{3.9}$$

where $\mathbf{r}_j$ are dimensionless vectors denoting the location of the ions, meaning that one can define an effective length scale, a, such that the actual location of the ions is $\mathbf{R}_j = a\mathbf{r}_j$. The parameter α is a dimensionless coefficient which sets the range of the interactions. In the limit $\alpha \to \infty$, the spins can be considered to be interacting only with their nearest neighbors. J sets the energy scale of the interaction. Within this work, I explore the effect on the maximum achievable squeezing by increasing α from zero to six. In previous works [14], spin squeezing on an arbitrary lattice for the OAT model has been analyzed, and the numerical simulations are compared to this work in appendix (A).

In addition to the two models discussed above, there is also a third Hamiltonian which generates squeezing. This is the so-called two-axis-counter-twisting model (abbreviated as TAC), which, although is considerably more difficult to realize experimentally, has been proposed to be realizable using dipole-dipole interactions between atoms in highly-excited electronic states in ref. [4]. The TAC model is governed by a Hamiltonian of the form:

$$\hat{H}_{TAC} = \sum_{j<k} \frac{J_{jk}}{2i} \left(\hat{\sigma}_j^+ \hat{\sigma}_k^+ - \hat{\sigma}_j^- \hat{\sigma}_k^- \right), \tag{3.10}$$

where $\hat{\sigma}_j^\pm = (1/2)\left(\hat{\sigma}_j^x \pm i\hat{\sigma}_j^y\right)$. The one-axis-twisting model achieves a variance in the spin com-

ponents transverse to the mean spin direction that scales with the number of spins, N, like $N^{1/3}$, while the two-axis-countertwisting achieves a variance in the transverse components that asymptotically approaches $1/2$ by increasing the number of spins [15]. Since the TAC model has a scaling of the variance that is smaller than the OAT model, the TAC model is expected to outperform the OAT model in terms of the maximum amount of achievable spin squeezing. In addition, another advantage of the TAC model is that the angle φ is constant in time.

The naming of the Hamiltonians hints at a geometrical interpretation of their effects. In the OAT model, consider first a CSS prepared with the mean spin direction aligned along the x-axis of the generalized Bloch sphere. The variance in the spin components perpendicular to the mean spin direction is isotropic, that is, $(\Delta S^y)^2 = (\Delta S^z)^2 = N/4$. Applying the one-axis-twisting Hamiltonian to this state will cause the probability distribution given by the Q-function to be sheared in the y-direction, as if the distribution was being twisted about the z-axis. This creates anisotropy between ΔS^y and ΔS^z, which leads to spin squeezing. Figure (3.2) illustrates this process.

In a similar manner, the two-axis-counter-twisting Hamiltonian has a geometrical interpretation, except that the mean spin direction is along the z-axis, and there are two axes which twist the probability distribution. The first axis is located at $\theta_1 = \pi/2, \phi_1 = \pi/4$, and the second is located at $\theta_2 = \pi/2, \phi_2 = -\pi/4$, and the two axes twist in opposite directions. This process is depicted in figure (3.3).

3.4 Time Evolution

The time evolution of the squeezing parameter is computed numerically using a *Mathematica* routine. At its heart, the simulation numerically solves the Schrödinger equation:

$$i\hbar\frac{\partial}{\partial t}\left|\psi(t)\right\rangle = \hat{H}\left|\psi(t)\right\rangle \tag{3.11}$$

using *Mathematica*'s `NDSolve` function for a given spin Hamiltonian. From this, the spin state obtained can be used to calculate all expectation values. Numerical methods are used because the

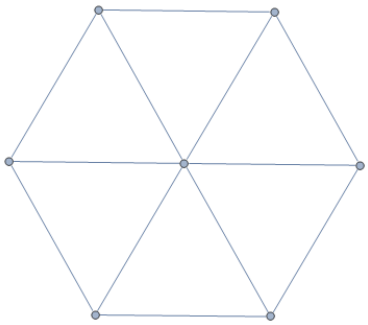

(a) Triangular lattice of effective spin-1/2 particles. There are seven total. Each particle is coupled to every other by the coupling constant J_{jk}.

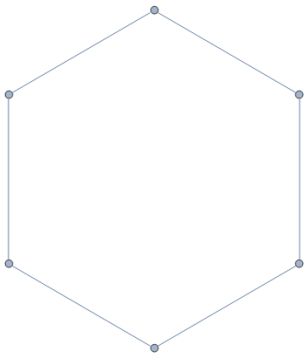

(b) Hexagonal lattice of effective spin-1/2 particles. In this case there are only six.

Figure 3.1: Lattice geometries

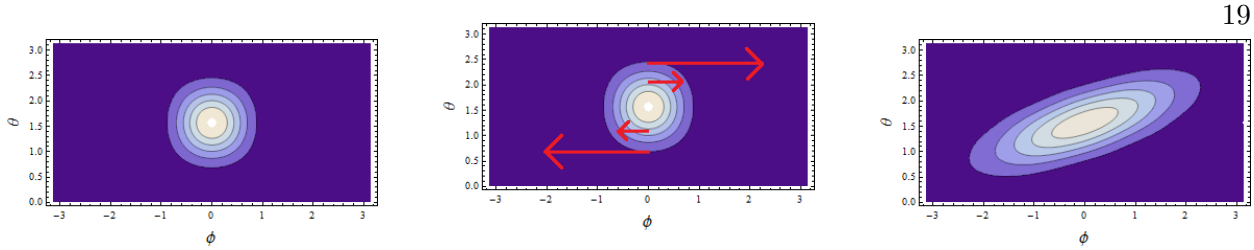

(a) Initial coherent state $\left|\frac{\pi}{2}, 0\right\rangle$

(b) Application of the one-axis-twisting Hamiltonian

(c) Resulting spin-squeezed state

Figure 3.2: Illustration of the effect of spin squeezing on the Q-function of a CSS with the one-axis-twisting Hamiltonian. In this figure, the Q-function is projected onto a two-dimensional domain

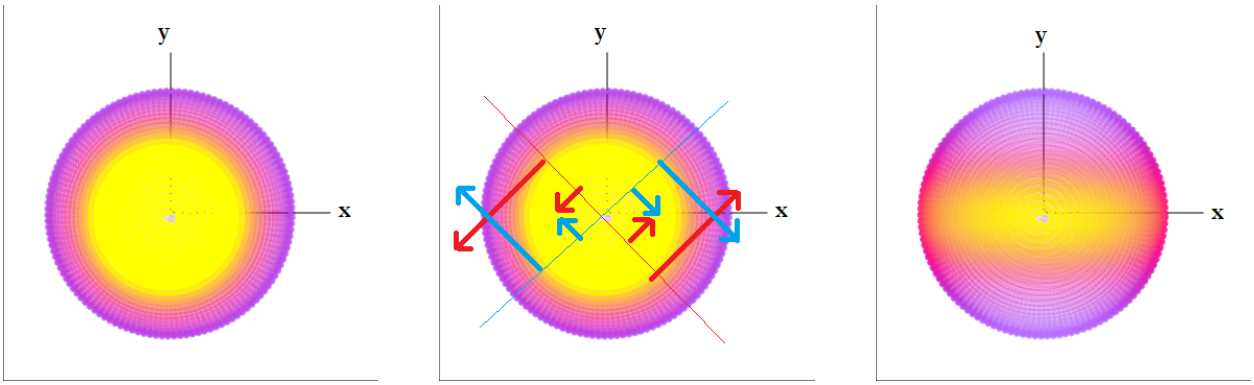

(a) (b) (c)

Figure 3.3: Illustration of the effect of spin squeezing on the Q-function of a CSS with the two-axis-counter-twisting Hamiltonian. In (a), the initial coherent state $|\theta = 0, \phi = 0\rangle$ is shown. In (b), we see the application of the two-axis-counter-twisting Hamiltonian. The red arrows are the shear generated by the twisting axis located at $\theta_1 = \pi/2, \phi_1 = \pi/4$. The blue arrows are the shear generated by the twisting axis located at $\theta_2 = \pi/2, \phi_2 = -\pi/4$. In (c), we see the resulting spin-squeezed state.

Hamiltonian is a $2^N \times 2^N$ matrix for N particles, which can take very long to diagonalize using analytical methods. The numerical methods have been compared to exact expressions for the one-axis-twisting Hamiltonian, and strong qualitative agreement between the two has been found (see appendix A). No other analytical expressions for the squeezing for the XY Hamiltonian or TAC Hamiltonian are currently known to this author.

The code employed in the simulations was partially completed by the time it was incorporated into being used for calculating the spin squeezing. Most importantly, the code responsible for creating the Hamiltonians for an arbitrary number of spins was already completed. This code was

adopted based on its efficiency to generate the Hamiltonians in a fairly short amount of time. What was left was to implement the initial coherent state, the expectation values, and expressions for the squeezing parameter, as well as the geometry of the system.

Chapter 4

Results

This chapter presents the maximal squeezing available for the three models using various interaction ranges. First, the results for each Hamiltonian are given. Then, a global comparison of the maximally attainable squeezing is given. In each case, the squeezing parameter versus time and the minimum over time of the squeezing parameter are given. The latter quantity is the maximum achievable spin squeezing.

4.1 Squeezing for the OAT Hamiltonian

The one-axis-twisting Hamiltonian has been studied extensively, so the results presented here serve as an example of the expected behavior of the squeezing versus the interaction range. In figure (4.2), the maximum squeezing attainable over all time for a given interaction range is plotted. For both the triangular lattice and the hexagonal lattice, the maximum squeezing decreases with the increase of the parameter α. This can be understood as follows: the interaction range is inversely proportional to the parameter α, so that $\alpha = 0$ implies that the interaction range is infinite. In this case, each particle becomes correlated with every other in the system, with a strength which is independent of its distance. With $\alpha = 6$, the particles still become correlated, however, the correlations are weighted heavily on the separation distance of the particles. This behavior is expected to carry over to other Hamiltonians examined in this thesis.

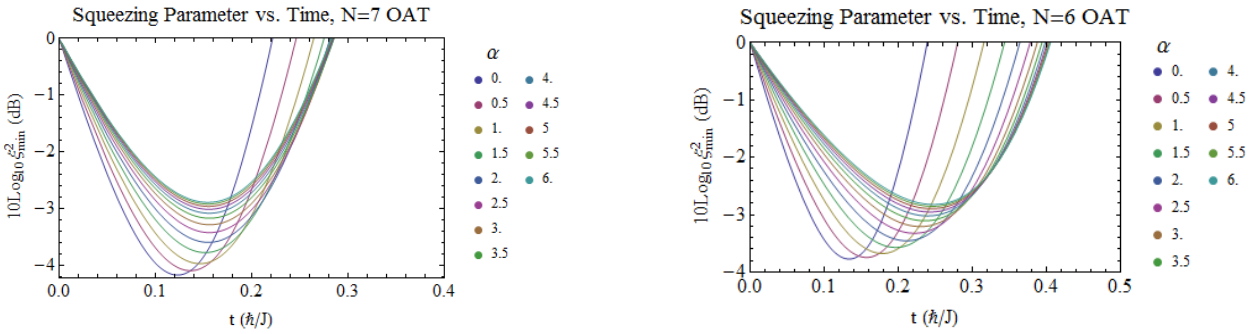

Figure 4.1: Time evolution of the squeezing parameters over the interaction range.

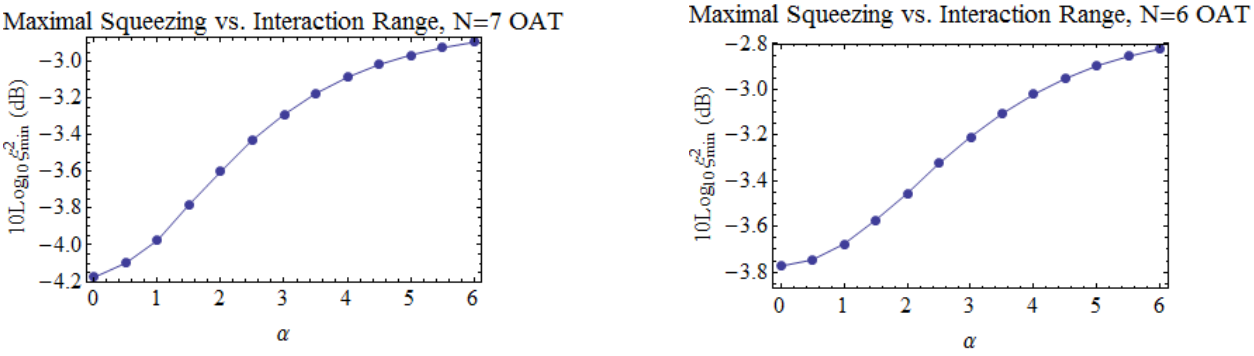

Figure 4.2: Maximal squeezing over time versus interaction range for the OAT Hamiltonian.

4.2 Squeezing for the XY Hamiltonian

The XY Hamiltonian is similar in behavior to the OAT Hamiltonian in that the maximal attainable squeezing over time is reduced as the interaction range decreases. The maximal attainable squeezing is given for $N = 7, \alpha = 0$ as -4.17625 dB, the same as for the OAT case. This is due to the fact that at $\alpha = 0$, the OAT and the XY Hamiltonians are the same up to an additive constant which does not induce squeezing. The results are summarized in figure (4.4), with the time evolution for each interaction range given in figure (4.3)

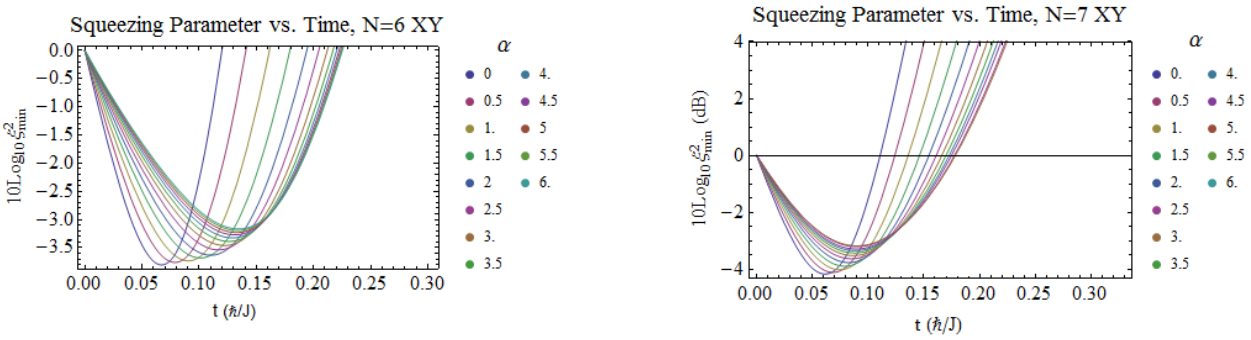

Figure 4.3: Time evolution of the squeezing parameters over the interaction range.

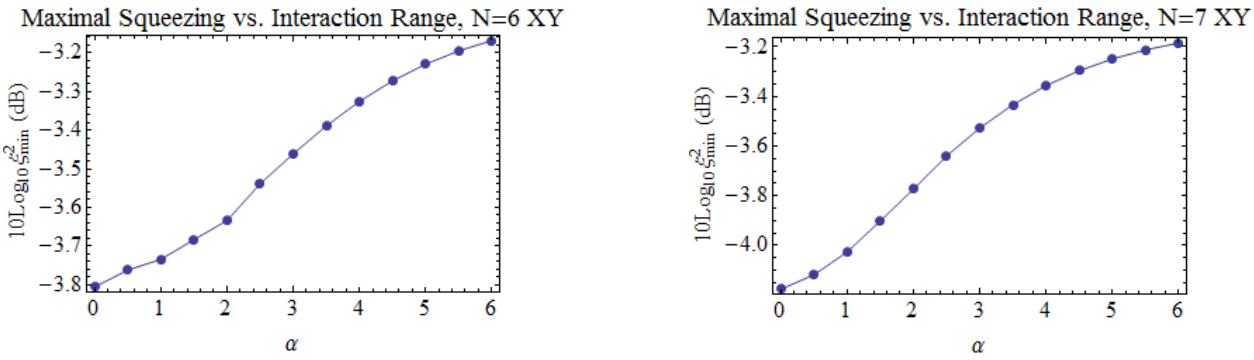

Figure 4.4: Maximal squeezing over time versus interaction range for the XY Hamiltonian.

4.3 Squeezing for the TAC Hamiltonian

The TAC Hamiltonian gives the maximal attainable squeezing for any given interaction range out of the three studied. The time to achieve this squeezing, however, is longer than the other two

models.

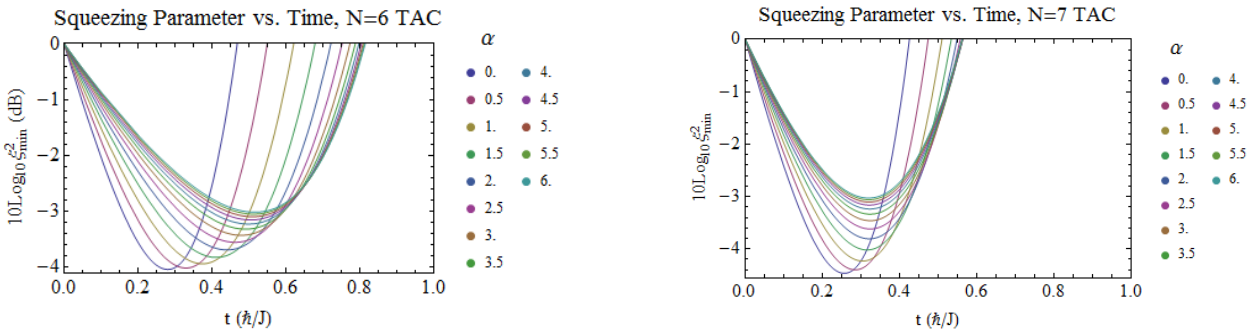

Figure 4.5: Time evolution of the squeezing parameters over the interaction range.

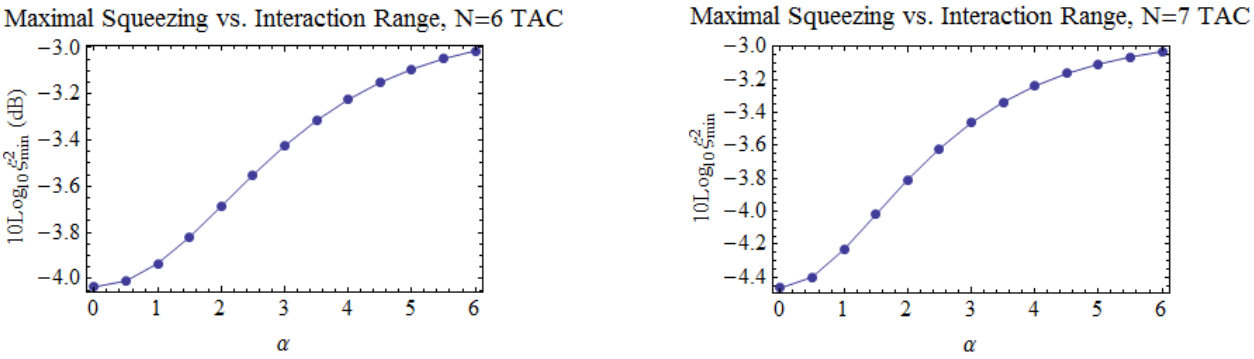

Figure 4.6: Maximal squeezing over time versus interaction range for the TAC Hamiltonian.

4.4 Maximum Squeezing

The maximum squeezing was found to be given by the TAC Hamiltonian at short ranges, and the XY Hamiltonian at long ranges, as can be seen in figure (4.7). The crossing occurs between $\alpha = 2$ and $\alpha = 3$.

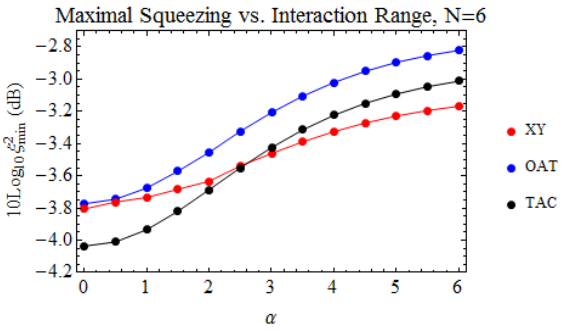

(a) Comparison of maximal attainable squeezing for all Hamiltonians investigated for six particles. Notice that the TAC Hamiltonian outperforms the others at short interaction ranges, but that XY achieves more squeezing for longer ranges.

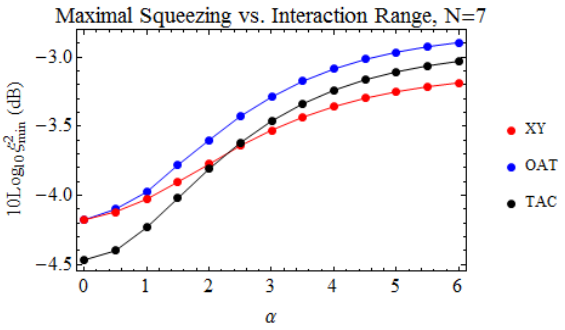

(b) Comparison of maximal attainable squeezing for all Hamiltonians investigated, for seven particles. The TAC Hamiltonian outperforms the others at short ranges, as for seven particles.

Figure 4.7: Maximal squeezing for all three models, for six or seven particles

Chapter 5

Conclusion and Outlook

The TAC Hamiltonian led to greater spin squeezing, but only at shorter ranges; the XY model led to greater spin squeezing at longer ranges. The maximum amount of squeezing found in this study was -4.4658dB for seven particles with all-to-all interaction range $\alpha = 0$.

5.1 Outlook

The methods presented herein have in no way exhausted the means by which one may generate spin squeezing, but merely analyzed a small subset of parameter ranges. The field of quantum control still has potential to find better ways to generate spin squeezing. For example, adding a transverse magnetic field to the OAT Hamiltonian promises to generate more squeezing that may last longer than the OAT Hamiltonian alone, which is shown in figure (5.1).

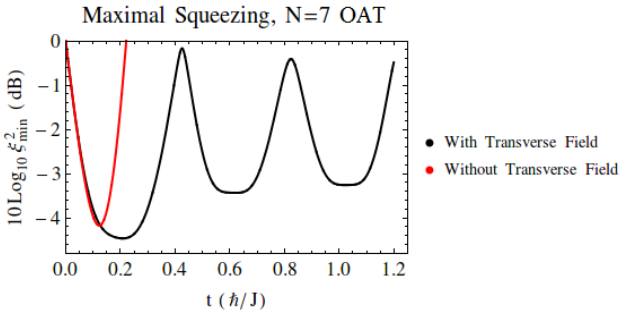

Figure 5.1: Comparison of OAT Hamiltonian with and without a transverse field

In addition, since the TAC Hamiltonian was found to take longer to bring about maximal squeezing, notions of the optimal squeezing rate have been studied in order to achieve the maximal

amount of squeezing in the shortest time [16].

So far, the notion of spin squeezing has been constrained to systems consisting of spin-1/2 particles. But as experimental accessibility improves, one could consider a system composed of spin-N particles and hope to generate spin squeezing. For example, systems of alkaline-earth atoms with emergent $SU(N)$ symmetries have been suggested [17] as a potential system to generate spin squeezing. The code presented within this thesis can be extended to these systems, with the caveat that the Hilbert spaces involved are much larger.

Therefore in conclusion, the simulations presented within this thesis serve both as an informative guide to spin squeezing in current atomic systems, and as a springboard towards future endeavors in the areas of precision metrology and quantum simulation with atomic systems.

Bibliography

[1] N Hinkley, J A Sherman, N B Phillips, M Schioppo, N D Lemke, K Beloy, M Pizzocaro, C W Oates, and A D Ludlow. An atomic clock with 10(-18) instability. Science (New York, N.Y.), 341(6151):1215–8, September 2013.

[2] Richard P. Feynman. Simulating physics with computers. International Journal of Theoretical Physics, 21(6-7):467–488, June 1982.

[3] Simcha Korenblit, Dvir Kafri, Wess C. Campbell, Rajibul Islam, Emily E. Edwards, Zhe-Xuan Gong, Guin-Dar Lin, Luming Duan, Jungsang Kim, Kihwan Kim, and Chris Monroe. Quantum Simulation of Spin Models on an Arbitrary Lattice with Trapped Ions. page 5, January 2012.

[4] Isabelle Bouchoule and Klaus Mø lmer. Spin squeezing of atoms by the dipole interaction in virtually excited Rydberg states. Physical Review A, 65(4):041803, April 2002.

[5] S Trotzky, P Cheinet, S Fölling, M Feld, U Schnorrberger, A M Rey, A Polkovnikov, E A Demler, M D Lukin, and I Bloch. Time-resolved observation and control of superexchange interactions with ultracold atoms in optical lattices. Science (New York, N.Y.), 319(5861):295–9, January 2008.

[6] D. Wineland, J. Bollinger, W. Itano, F. Moore, and D. Heinzen. Spin squeezing and reduced quantum noise in spectroscopy. Physical Review A, 46(11):R6797–R6800, December 1992.

[7] Peter Lambropoulos and David Petrosyan. Fundamentals of Quantum Optics and Quantum Information. Springer Berlin Heidelberg, Berlin, Heidelberg, 2007.

[8] Gretchen K Campbell and William D Phillips. Ultracold atoms and precise time standards. Philosophical transactions. Series A, Mathematical, physical, and engineering sciences, 369(1953):4078–89, October 2011.

[9] Jian Ma, Xiaoguang Wang, C.P. Sun, and Franco Nori. Quantum spin squeezing. Physics Reports, 509(2-3):89–165, December 2011.

[10] J. Bollinger, Wayne Itano, D. Wineland, and D. Heinzen. Optimal frequency measurements with maximally correlated states. Physical Review A, 54(6):R4649–R4652, December 1996.

[11] Masahiro Kitagawa and Masahito Ueda. Squeezed spin states. Physical Review A, 47(6):5138–5143, June 1993.

[12] Duger Ulam-Orgikh and Masahiro Kitagawa. Spin squeezing and decoherence limit in Ramsey spectroscopy. Physical Review A, 64(5):052106, October 2001.

[13] V. Meyer, M. Rowe, D. Kielpinski, C. Sackett, W. Itano, C. Monroe, and D. Wineland. Experimental Demonstration of Entanglement-Enhanced Rotation Angle Estimation Using Trapped Ions. Physical Review Letters, 86(26):5870–5873, June 2001.

[14] M Foss-Feig, K R A Hazzard, J J Bollinger, A M Rey, and C W Clark. Dynamical quantum correlations of Ising models on an arbitrary lattice and their resilience to decoherence. New Journal of Physics, 15(11):113008, November 2013.

[15] S. Huelga, C. Macchiavello, T. Pellizzari, A. Ekert, M. Plenio, and J. Cirac. Improvement of Frequency Standards with Quantum Entanglement. Physical Review Letters, 79(20):3865–3868, November 1997.

[16] Tomas Opatrny. Dynamical spin squeezing: combining fast one-axis twisting and deep two-axis counter-twisting. page 4, September 2014.

[17] Miguel a Cazalilla and Ana Maria Rey. Ultracold Fermi Gases with Emergent SU(N) Symmetry. arXiv, page 43, March 2014.

[18] Immanuel Bloch. Ultracold quantum gases in optical lattices. Nature Physics, 1(1):23–30, October 2005.

[19] E. C. Bulllard. An Atomic Standard of Frequency and Time Interval: Definition of the Second of Time. Nature, 176(4476):282–282, August 1955.

[20] L.-M. Duan. Effective Hamiltonian for Fermions in an Optical Lattice across a Feshbach Resonance. Physical Review Letters, 95(24):243202, December 2005.

[21] D. Meiser, Jun Ye, and M. J. Holland. Spin squeezing in optical lattice clocks via lattice-based QND measurements. July 2007.

[22] Tomáš Opatrný. Twisting tensor and spin squeezing. page 5, August 2014.

[23] Norman Ramsey. A Molecular Beam Resonance Method with Separated Oscillating Fields. Physical Review, 78(6):695–699, June 1950.

[24] Ana Maria Rey. Ultracold Bosonic Atoms in Optical Lattices, 2004.

[25] Franz Schwabl. Advanced Quantum Mechanics. Springer Berlin Heidelberg, Berlin, Heidelberg, 4th edition, 2008.

[26] Giuseppe Vitagliano, Iagoba Apellaniz, Iñigo L. Egusquiza, and Géza Tóth. Spin squeezing and entanglement for an arbitrary spin. Physical Review A, 89(3):032307, March 2014.

Appendix A

Derivation of Relevant Squeezing Parameters

A.1 Derivation of ξ

This section provides the derivation of the squeezing parameter, ξ^2. From the definition, we have

$$\xi = \frac{min\left(\Delta\left(\mathbf{S}\cdot\mathbf{n}_{\perp}\right)\right)}{|\langle\mathbf{S}\rangle|} \tag{A.1}$$

$$min\left(\Delta\left(\mathbf{S}\cdot\mathbf{n}_{\perp}\right)\right) = min\left(\left\langle\left(\mathbf{S}\cdot\mathbf{n}_{\perp}\right)^2\right\rangle - \langle(\mathbf{S}\cdot\hat{n}_{\perp})\rangle^2\right). \tag{A.2}$$

Assuming that the mean spin direction is along the x-axis of the generalized Bloch sphere, the first step to finding the minimum of the quantity $\Delta\left(\mathbf{S}\cdot\mathbf{n}_{\perp}\right)$ is to parameterize the normalized vector $\mathbf{n}_{\perp}$ in terms of the two vectors, $\mathbf{y}$ and $\mathbf{z}$, which point perpendicular to the mean spin direction, and an angle φ such that:

$$\mathbf{n}_{\perp} = \cos(\varphi)\mathbf{y} + \sin(\varphi)\mathbf{z} \tag{A.3}$$

Upon substitution, the variance perpendicular to the mean spin direction is given by:

$$\left(\Delta\left(\mathbf{S}\cdot\mathbf{n}_{\perp}\right)\right)^2 = \left(\Delta S^y\right)^2\cos^2(\varphi) + \left(\Delta S^z\right)^2\sin^2(\varphi) + \left(\frac{1}{2}\left\langle\{S^y, S^z\}\right\rangle - \left\langle S^y\right\rangle\left\langle S^z\right\rangle\right)\sin(2\varphi) \tag{A.4}$$

$$\Longrightarrow \xi^2 = \frac{min\left(\Delta S^y\right)^2\cos^2(\varphi) + \left(\Delta S^z\right)^2\sin^2(\varphi) + \left(\frac{1}{2}\left\langle\{S^y, S^z\}\right\rangle - \left\langle S^y\right\rangle\left\langle S^z\right\rangle\right)\sin(2\varphi)}{|\langle\mathbf{S}\rangle|^2}, \tag{A.5}$$

where $\{\hat{S}^y, \hat{S}^z\}$ is the anticommutator, $\hat{S}^y\hat{S}^z + \hat{S}^z\hat{S}^y$. Since the square root function is monotonic increasing, then finding the minimum of ξ^2 is equivalent to finding the minimum of ξ.

A.2 Derivation of φ

The squeezing parameter is minimized with respect to the angle, φ, which parameterizes the vector $\mathbf{n}_\perp$. This means that there is a special angle φ_0 such that

$$\left.\frac{\partial}{\partial\varphi}\right|_{\varphi_0} \xi = 0 \tag{A.6}$$

Evaluating the derivative and solving for φ_0 is straightforward:

$$\frac{\partial\xi^2}{\partial\varphi} = \frac{-\left(\Delta S^y\right)^2\sin(2\varphi) + \left(\Delta S^z\right)^2\sin(2\varphi) + \left(\frac{1}{2}\left\langle\{S^y,S^z\}\right\rangle - \left\langle S^y\right\rangle\left\langle S^z\right\rangle\right)2\cos(2\varphi)}{\left|\langle\mathbf{S}\rangle\right|^2} \tag{A.7}$$

$$\Longrightarrow \frac{-\left(\Delta S^y\right)^2\sin(2\varphi_0) + \left(\Delta S^z\right)^2\sin(2\varphi_0) + \left(\frac{1}{2}\left\langle\{S^y,S^z\}\right\rangle - \left\langle S^y\right\rangle\left\langle S^z\right\rangle\right)2\cos(2\varphi_0)}{\left|\langle\mathbf{S}\rangle\right|^2} = 0 \tag{A.8}$$

$$\Longrightarrow \left(\Delta S^y\right)^2\sin(2\varphi_0) - \left(\Delta S^z\right)^2\sin(2\varphi_0) = \left(\frac{1}{2}\left\langle\{S^y,S^z\}\right\rangle - \left\langle S^y\right\rangle\left\langle S^z\right\rangle\right)2\cos(2\varphi_0) \tag{A.9}$$

$$\tan(2\varphi_0) = \left(\frac{\left\langle\{S^y,S^z\}\right\rangle - 2\left\langle S^y\right\rangle\left\langle S^z\right\rangle}{\left(\Delta S^y\right)^2 - \left(\Delta S^z\right)^2}\right) \tag{A.10}$$

$$\Longrightarrow \varphi_0 = \frac{1}{2}\tan^{-1}\left[\frac{2\left\langle S^y\right\rangle\left\langle S^z\right\rangle - \left\langle\{S^y,S^z\}\right\rangle}{\left(\Delta S^z\right)^2 - \left(\Delta S^y\right)^2}\right] \tag{A.11}$$

By setting $\varphi = \varphi_0$ in the expression for the squeezing parameter, the squeezing parameter is minimized with respect to φ.

A.3 Coupling Strength Matrices

Presented in this section is an explicit form for the coupling matrices $J_{jk} = \frac{1}{|\mathbf{r}_j - \mathbf{r}_k|^\alpha}$ used in the numerical calculations. For seven particles, the matrix with $\alpha = 1$:

$$J = \begin{pmatrix} 0 & 1 & \frac{1}{\sqrt{3}} & \frac{1}{2} & \frac{1}{\sqrt{3}} & 1 & 1 \\ 1 & 0 & 1 & \frac{1}{\sqrt{3}} & \frac{1}{2} & \frac{1}{\sqrt{3}} & 1 \\ \frac{1}{\sqrt{3}} & 1 & 0 & 1 & \frac{1}{\sqrt{3}} & \frac{1}{2} & 1 \\ \frac{1}{2} & \frac{1}{\sqrt{3}} & 1 & 0 & 1 & \frac{1}{\sqrt{3}} & 1 \\ \frac{1}{\sqrt{3}} & \frac{1}{2} & \frac{1}{\sqrt{3}} & 1 & 0 & 1 & 1 \\ 1 & \frac{1}{\sqrt{3}} & \frac{1}{2} & \frac{1}{\sqrt{3}} & 1 & 0 & 1 \\ 1 & 1 & 1 & 1 & 1 & 1 & 0 \end{pmatrix}, \tag{A.12}$$

whereas for six particles the matrix with $\alpha = 1$ is

$$J = \begin{pmatrix} 0 & 1 & \frac{1}{\sqrt{3}} & \frac{1}{2} & \frac{1}{\sqrt{3}} & 1 \\ 1 & 0 & 1 & \frac{1}{\sqrt{3}} & \frac{1}{2} & \frac{1}{\sqrt{3}} \\ \frac{1}{\sqrt{3}} & 1 & 0 & 1 & \frac{1}{\sqrt{3}} & \frac{1}{2} \\ \frac{1}{2} & \frac{1}{\sqrt{3}} & 1 & 0 & 1 & \frac{1}{\sqrt{3}} \\ \frac{1}{\sqrt{3}} & \frac{1}{2} & \frac{1}{\sqrt{3}} & 1 & 0 & 1 \\ 1 & \frac{1}{\sqrt{3}} & \frac{1}{2} & \frac{1}{\sqrt{3}} & 1 & 0 \end{pmatrix}. \tag{A.13}$$

A.4 Analytic Comparison of Spin Squeezing Quantities

Using the expressions from ref. [14], it is possible to do an analytical treatment of the squeezing in the case for the OAT Hamiltonian. The relevant quantities to calculate are presented

below, with $\hbar \to 1$

$$\langle S^x \rangle = \frac{1}{2} \sum_j \langle \hat{\sigma}_j^x \rangle \tag{A.14}$$

$$\langle S^y \rangle = \frac{1}{2} \sum_j \left\langle \hat{\sigma}_j^y \right\rangle \tag{A.15}$$

$$\langle S^z \rangle = \frac{1}{2} \sum_j \langle \hat{\sigma}_j^z \rangle \tag{A.16}$$

$$\left\langle (S^y)^2 \right\rangle = \frac{1}{4} \sum_j \left\langle \left(\hat{\sigma}_j^y \right)^2 \right\rangle + \frac{1}{4} \sum_{j \neq k} \left\langle \hat{\sigma}_j^y \hat{\sigma}_k^y \right\rangle \tag{A.17}$$

$$\left\langle (S^z)^2 \right\rangle = \frac{1}{4} \sum_j \left\langle \left(\hat{\sigma}_j^z \right)^2 \right\rangle + \frac{1}{4} \sum_{j \neq k} \langle \hat{\sigma}_j^z \hat{\sigma}_k^z \rangle \tag{A.18}$$

$$\langle S^y S^z \rangle = \frac{i}{4} \sum_j \langle \hat{\sigma}_j^x \rangle + \frac{1}{4} \sum_{j \neq k} \left\langle \hat{\sigma}_j^y \hat{\sigma}_k^z \right\rangle \tag{A.19}$$

$$\langle S^z S^y \rangle = -\frac{i}{4} \sum_j \langle \hat{\sigma}_j^x \rangle + \frac{1}{4} \sum_{j \neq k} \langle \hat{\sigma}_j^z \hat{\sigma}_k^y \rangle \tag{A.20}$$

In each case examined (e.g. with six or seven particles), the agreement between the theory and the numberical computation has proved to be qualitatively similar. Presented in figure (A.1) are plots of the agreement between the two calculations.

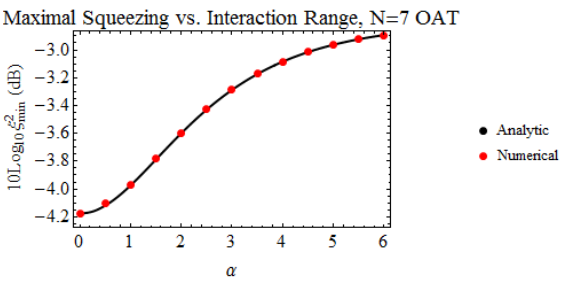

(a) Comparison of theory (black) with numerical calculations (red) for the OAT Hamiltonian and seven particles.

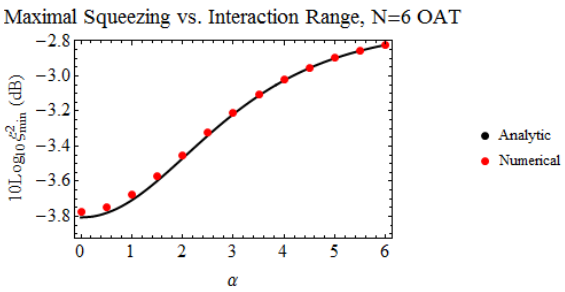

(b) Comparison of theory (black) with numerical calculations (red) for the OAT Hamiltonian and six particles.

Figure A.1: Comparison of analytical treatment and numerical simulations